Ore Geology Reviews 162 (2023) 105685

Contents lists available at ScienceDirect

Ore Geology Reviews

journal homepage: www.elsevier.com/locate/oregeorev

Lithium enrichment of the magmatic-hydrothermal fluid in albite-spodumene pegmatite from Lijiagou, Eastern Tibetan Plateau: Evidence from fluid inclusions

Yabin Yuan [a,b,*], Bin Chen [b,*], Linbo Shang [c], Eszter Sendula [d], I-Ming Chou [a]

[a] CAS Key Laboratory of Experimental Study under Deep-sea Extreme Conditions, Institute of Deep-sea Science and Engineering, Chinese Academy of Sciences, Sanya, Hainan 572000, China
[b] Department of Earth and Space Sciences, Southern University of Science and Technology, Shenzhen 518055, China
[c] State Key Laboratory of Ore Deposit Geochemistry, Institute of Geochemistry, Chinese Academy of Sciences, Guiyang 550081, China
[d] Department of Geosciences, UiT – The Arctic University of Norway, N-9037 Tromsø, Norway

ARTICLE INFO

Keywords:
Albite-spodumene pegmatite
LCT pegmatite
Fluid inclusions
Li enrichment in magmatic-hydrothermal fluid
Lijiagou deposit

ABSTRACT

Albite-spodumene pegmatites, which are remarkable resources of Li worldwide, may experience both magmatic-hydrothermal transition and sub-solidus hydrothermal alteration during their formation and evolution. However, fluids involved in the different stages of the evolution of a spodumene-bearing pegmatitic systems are not well defined, especially at the magmatic-hydrothermal transition stage. In the Lijiagou deposit, western Sichuan Province, fluid inclusions of a typical albite-spodumene pegmatite were studied to determine the degree of magmatic-hydrothermal fluid Li enrichment and the potential for lithium mineral crystallization at the magmatic-hydrothermal transition stage.

Micro-petrographic analyses identified different types of fluid inclusions of either primary, pseudo-secondary or secondary origin and inclusions containing devitrified silicate glass. The presence of these inclusions suggests that the pegmatite underwent both the magmatic-hydrothermal transition stage and a post-crystallization hydrothermal process over its evolution. The results of fluid inclusion LA-ICP-MS analyses show that the aqueous ± carbonic fluids represented by the pseudo-secondary type 1a and 1b inclusions carry significant amount of Li, with Na and Li predominating the cation budget of these pegmatitic fluids. The aqueous ± carbonic fluids exhibit typical magmatic-hydrothermal fluid compositional characteristics and exhibit high abundance of Li in this pegmatitic system at the magmatic-hydrothermal transition stage. The relative abundance of Li to Na and K lies within the uppermost range of those reported from lithium-cesium-tantalum pegmatite systems. This is consistent with the elevated incorporation of Li in pegmatitic quartz from the albite-spodumene pegmatite. The compositional characteristics of the fluids at the magmatic-hydrothermal transition stage may be used to imply the Li mineralization potential of the pegmatitic system.

1. Introduction

Rare-element pegmatites, a remarkable resource of rare metals (such as Li, Be, Nb, Ta) around the world are generally enriched in rare-element minerals (beryl, spodumene, tantalite, etc.) (London, 2014). The possible factors of rare element mineralization in the pegmatitic system have been long studied including the effects of the magma source, the magmatic and hydrothermal evolution process, and the sub-solidus hydrothermal alteration (Simmons & Webber, 2008; Chen et al., 2020). Although several mechanisms of the pegmatite crystallization process, such as liquid immiscibility (Thomas & Davidson, 2006) and constitutional zonation refining (London, 2014), have been put forward as critical factors in forming rare-element pegmatites, the sub-solidus alteration is also considered as one of the major causes for rare element mineralization (Černý et al., 1998; Burns, 2016; Liu et al., 2020). In general, elevated Li concentration in the pegmatitic system has been considered to not only promote the crystallization of spodumene, but as a fluxing component contributing to lowering the crystallization temperature below the equilibrium solidus of silicate melts which benefits the formation of pegmatitic structure (Gammel & Nabelek, 2016).

* Corresponding authors.
E-mail addresses: yuanyb@idsse.ac.cn (Y. Yuan), chenb6@sustech.edu.cn (B. Chen).

https://doi.org/10.1016/j.oregeorev.2023.105685
Received 6 March 2023; Received in revised form 17 September 2023; Accepted 18 September 2023
Available online 19 September 2023

The high abundance of Li in the system was usually indicated by the bulk composition and mineral elemental composition of the pegmatite (Roda-Robles et al., 1995; Maloney et al., 2008; Potter et al., 2009). However, as hydrothermal metasomatism is often reported to occur in Li-mineralized pegmatites (Kaeter et al., 2018), it is unclear if the estimated Li concentration in the pegmatitic rock based on the bulk and mineral composition is representative of the Li abundance in the system over the pegmatite crystallization process. Moreover, the coarse and variable grain size makes the obtained bulk composition of pegmatite uncertain (Yuan et al., 2021). The formation of rare-element pegmatite is generally considered to have experienced the magmatic-hydrothermal transition stage, which has been recorded by the melt and fluid inclusions trapped in pegmatite minerals (Rickers et al., 2006; Thomas & Davidson, 2016; Hulsbosch et al., 2019). Moreover, melt and fluid inclusions entrapped during pegmatite crystallization hold reliable information on the compositional characteristic of the pegmatitic system and is thereby commonly used for indicating the geochemical behavior of rare elements (Audétat & Pettke, 2003; Zajacz et al., 2008; Sirbescu et al., 2013; Hulsbosch et al., 2019).

Among the Li-mineralized pegmatites, albite-spodumene type supplies significant Li production around the world (Grew, 2020). This type of pegmatitic rock is characterized by the dominance of quartz and albite over K-feldspar besides containing spodumene, with the bulk pegmatite Li concentration being around 2 wt% Li_2O which is within the uppermost range obtained by the experimental enrichment of magmatic Li (Stewart, 1978; Cerny & Ercit, 2005; Barros, et al., 2020). However, the natural Li abundance in the pegmatitic fluid at the magmatic-hydrothermal transition stage during the albite-spodumene pegmatite formation is rarely known.

In the Ke'eryin area, western Sichuan Province, several giant pegmatite-type Li deposits (e.g., Lijiagou, Dangba) have been investigated with the total Li_2O reserve of>500,000 tons and the albite-spodumene pegmatite is the major type aimed for Li exploration in this region (Gu, 2014). In this study, a typical albite-spodumene type pegmatite in the Lijiagou deposit was investigated and the pegmatitic fluid characteristics at the magmatic-hydrothermal transition stage were constrained using fluid inclusions. Previously, the fluid inclusion types and related properties were classified for constraining the fluid characteristics in this mineralized pegmatitic system (Fei et al., 2021). However, the exact composition of the fluid, particularly at the magmatic-hydrothermal transition stage is still unknown, making the mineralization process obscure. Here, the composition and other properties (e.g., density, salinity) of the fluids trapped during the pegmatite formation were determined using a combination of methods such as fluid inclusion micropetrography, microthermometry, and single fluid inclusion LA-ICP-MS analyses. The enrichment degree of Li in the pegmatitic fluids of the albite-spodumene system was compared to previously reported fluid compositional data from different types of pegmatitic systems, placing this deposit to the uppermost range of LCT pegmatites based on Li/Na and Li/K ratios.

2. Geological background

The Ke'eryin area, western Sichuan Province of China, is located at the eastern part of the Songpan-Ganze Orogenic Belt (SGOB) which lies between the Kunlun-Qaidam terrane to the north and Qiangtang terrane to the south, and neighbors with the Yangtze terrane to the east (Fig. 1). The eastern SGOB is largely composed of the Neoproterozoic crystalline complex, an overlying sequence of Triassic turbidite deposits, and Triassic to Jurassic igneous rocks (Xu et al., 2020). The Triassic turbiditic metasedimentary rock sequence of this region is also known as the Xikang Group which includes the Zagunao Formation, Zhuwo Formation and Xinduqiao Formation. The turbiditic sequence mainly consists of *meta*-felsic sandstone, *meta*-siltstone, sericite slate, silty slate, phyllite, schist, and a minor amount of limestone. The metasedimentary rock sequence is the country rock for numerous early Mesozoic plutons and pegmatites (Weislogel et al., 2010). The granitic intrusive rocks in the eastern SGOB region formed during the Triassic and Jurassic periods (ages range between 228 Ma and 195 Ma) and include high-K calc-alkaline granites to granodiorites, high-K alkaline granites and peraluminous S-type granites (Zhao et al., 2022).

In the Ke'eryin area, the plutons intruding into the Xikang Group are Triassic to Jurassic granitoids with an area of ~ 250 km^2, and the lithologies include quartz diorite, biotite monzogranite, muscovite albite granite, biotite moyite and two-mica granite (Fig. 2a). The pegmatites are mostly intruded into the metasedimentary rock and partly into the granitic pluton and were formed at 211–200 Ma (Fei et al., 2020). The pegmatites are spatially distributed in or around the Ke'eryin granite

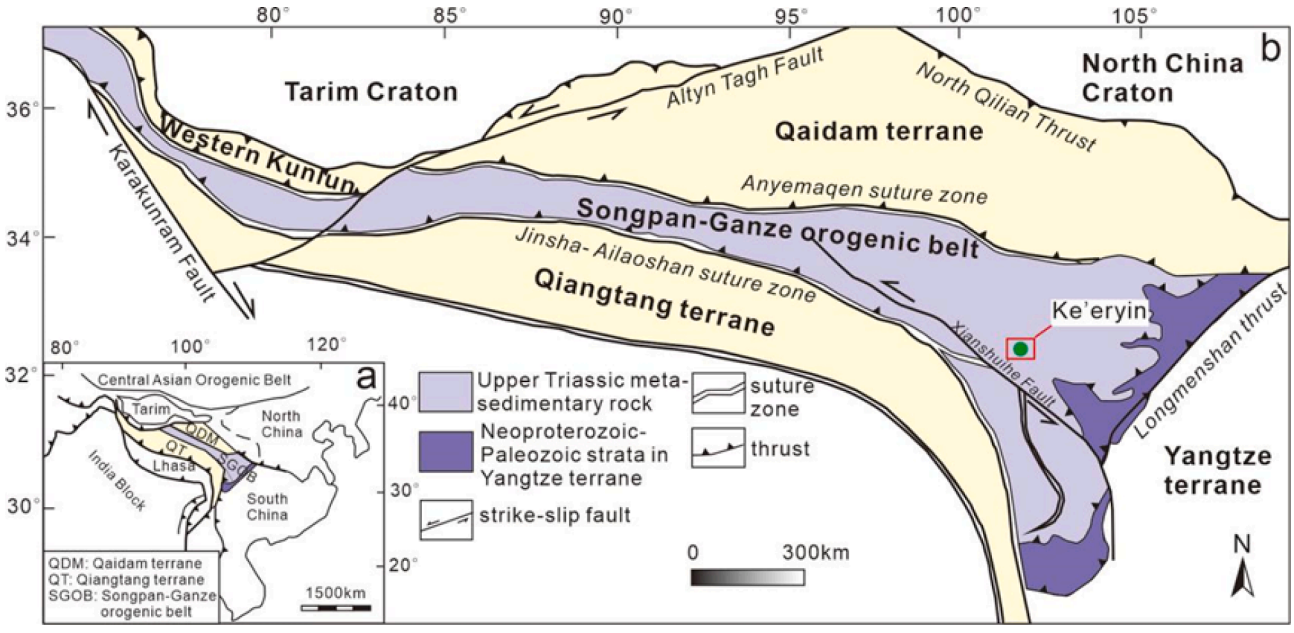

Fig. 1. (a) The location of the Songpan-Ganze orogenic belt in the northern Tibetan Plateau (after Zhao et al., 2022). (b) Geological map of the Songpan-Ganze orogenic belt with the location of the Ke'eryin study area (modified after Xu et al., 2020).

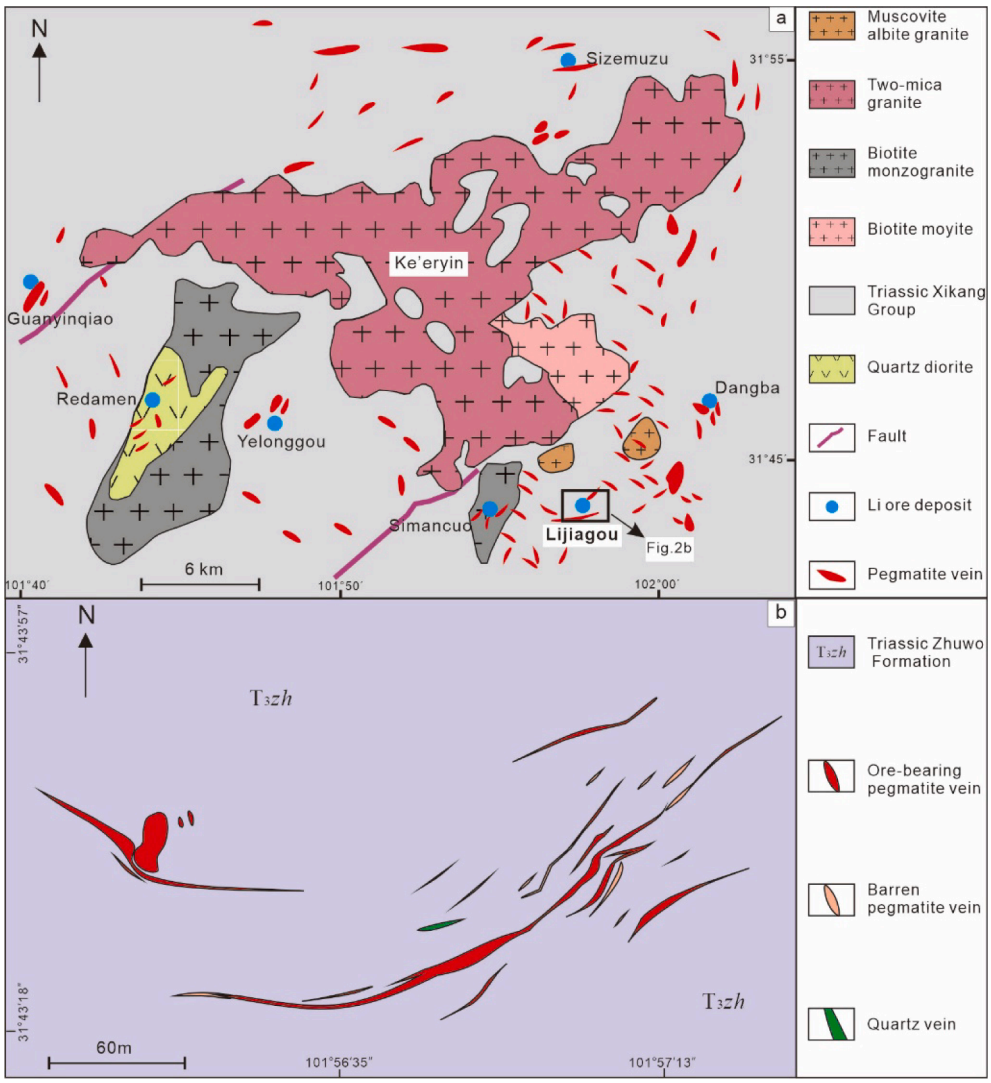

Fig. 2. Geological map of (a) the Ke'eryin area and (b) the Lijiagou deposit located in the southeast part of the Ke'eryin area (modified after Fei et al., 2020). Most of the Li-mineralized pegmatite veins are 15–30 m thick and are generally thicker than the barren pegmatite veins in the deposit (Gu, 2014; Liao et al., 2019).

pluton. In total, five igneous rock zones were defined with increasing distance from the pluton according to the mineralogical composition: (I) two-mica granite and microcline pegmatite, (II) microcline-albite pegmatite; (III) albite pegmatite, (IV) albite-spodumene pegmatite and (V) lepidolite pegmatite (Li et al., 2006; Fei et al., 2020). Although it has traditionally been considered that the pegmatite in this area was formed by the extended fractional crystallization of the granitic magmas (Li, 2006), the recent study of ore forming fluid evolution indicates that each type of pegmatite was formed by separate anatexis (Fei et al., 2021). Among these, the albite-spodumene and the lepidolite types are the main mineralized pegmatites for the purpose of Li exploration, with the albite-spodumene type accounting for 95% of the Li-mineralized pegmatites in this area (Liao et al., 2019). A series of pegmatite-related Li deposits occur in this area, such as the Lijiagou, Dangba, Sizemuzu, Simancuo, Yelonggou, Remenda, and Guanyinqiao deposits which constitute the Ke'eryin ore field (Fig. 2a).

The Lijiagou deposit which has the Li resource of ~ 0.51 Mt, is one of the biggest reported ore deposits in the area (Fei et al., 2020). We focused our study on the albite-spodumene pegmatite from this deposit. Outcrops in the Lijiagou deposit include Triassic *meta*-sedimentary rocks and Quaternary sediments. The series of *meta*-sedimentary rocks is called the Upper Triassic Zhuwo Formation (T_3zh) and comprise mainly of hornfels and leptynite (Fei et al., 2020). The hornfels include quartz hornfels, felsic hornfels, two-mica hornfels, diopside hornfels, garnet quartz hornfels, and biotite hornfels and the leptynite consists of two-mica and biotite leptynites. The intrusive rocks such as pegmatite dikes, aplite and quartz veins occur in an area where granite outcrops are barely present (Fig. 2b). Approximately 85 pegmatite dikes have been located in the deposit, including albite, lepidolite, and albite-spodumene type pegmatites. These pegmatite dikes emplaced either concordantly or discordantly to the metasedimentary bedding. The albite-spodumene type pegmatite commonly shows no zonation (Fig. 3a) or is weakly zoned from the edge of the dike towards the center (Fig. 3b), with an aplite zone occurring at the margin that is mainly composed of fine-grained muscovite, quartz, microcline, albite, and in some cases garnet, tourmaline and spodumene. The minerals in the inner part of the dikes are generally show heterogeneous distribution and a coarser grain size, and mainly include quartz, albite, spodumene and microcline.

3. Sample description

Samples were collected from an outcrop of an approximately 9 m wide albite-spodumene pegmatite dike in the Lijiagou deposit. This dike contains an outer zone of aplite and an inner zone containing medium to coarse grained minerals with varying proportions at different sites. Rock

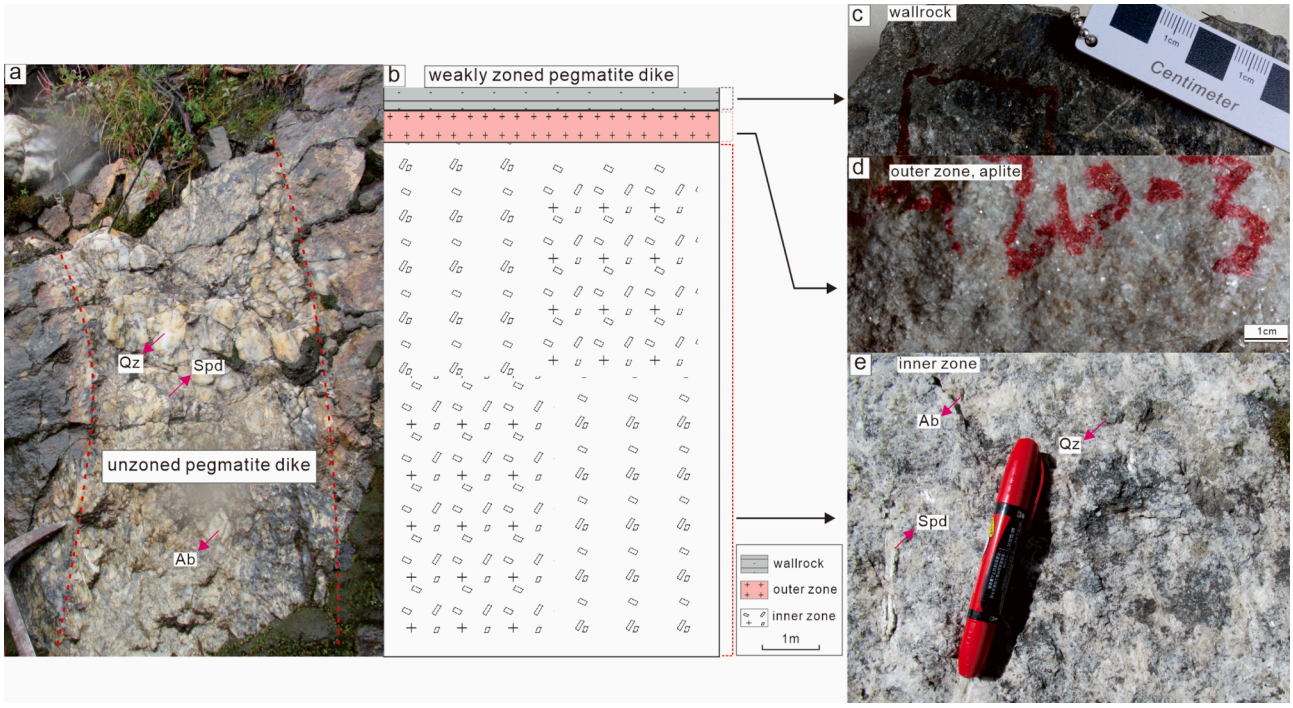

Fig. 3. (a) Photo of the albite-spodumene pegmatite dike intruding into the wall-rock of hornfels and showing no zonation. (b) A simplified sketch of the albite-spodumene pegmatite dike showing weak internal zonation. It includes an outer zone with fine-grained mineral assemblages and an inner zone containing coarser minerals. (c) Photo of a representative rock sample from the *meta*-sandstone wall-rock. (d) Representative rock sample from the outer aplite zone adjacent to the wall-rock. (e) Representative rock sample from the inner zone with coarse-grained minerals including albite (Ab), spodumene (Spd) and quartz (Qz).

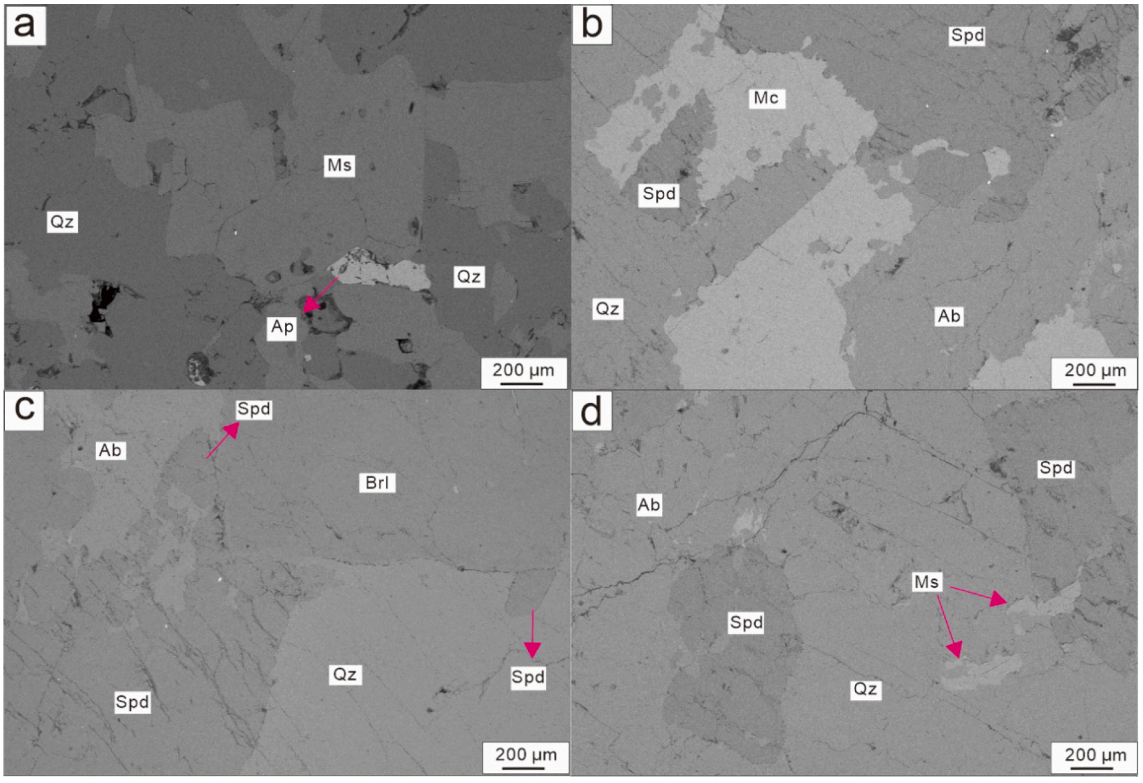

Fig. 4. Backscattered electron (BSE) images of (a) the aplite sample from the outer zone of the dike with a mineral assemblage including quartz, muscovite, albite and apatite, and (b-d) rock samples from the Li-mineralized inner zone of the dike. (b) The major mineral phases in the inner zone are quartz, microcline, albite and spodumene. (c) Partially albitised spodumene and beryl was observed to be intergrown with spodumene and quartz. (d) Partially muscovitised spodumene. Abbreviations: Ab–albite, Ap–apatite, Brl–beryl, Mc–microcline, Ms–muscovite, Qz–quartz, Spd–spodumene.

samples from both the inner and the outer zones were collected. The aplite is ~ 50 cm thick and occurs at the border of the pegmatite dike and the wall rock (Fig. 3b-d). It is mainly composed of fine-grained (0.5–1.5 mm) anhedral quartz (35–45 vol%), muscovite (35–45 vol%), apatite (5–15 vol%), and minor amounts of tourmaline, beryl, and albite (Fig. 4a). In the ~ 8.5 m wide inner zone (Fig. 3b) the major mineral phases are predominantly subhedral and medium to coarse grained (mm-dm) albite (20–40 vol%), quartz (20–30 vol%), microcline (15–30 vol%), spodumene (10–30 vol%), and muscovite (5–10%) (Fig. 3e, 4b), with minor amounts of beryl, apatite and other accessory minerals present. Both feldspar and quartz generally show tabular or irregular shape. Spodumene crystals commonly display elongated shape and unidirectional solidification texture. Though in many cases the spodumene is intergrown with quartz, albite, and microcline, indication of metasomatic alteration of spodumene such as albitization or muscovitization is occasionally present (Fig. 4c, d).

4. Analytical methods

4.1. Fluid inclusion petrography and microthermometry

Several doubly polished thick sections were prepared from samples collected in both the outer and the inner zones of the pegmatite dike to study fluid inclusions (FI) in different host minerals. Fluid inclusion petrography was performed using a Zeiss Axio Scope. A1 light microscope (Carl Zeiss, Germany) in the fluid inclusion laboratory at the Southern University of Science and Technology.

Microthermometric analysis of fluid inclusions was carried out at the State Key Laboratory of Ore Deposit Geochemistry, Chinese Academy of Sciences. The analysis was conducted with a Linkam THMSG 600 heating-freezing stage which has been calibrated using synthetic fluid inclusions of known composition. The measured temperatures are considered to be accurate to ± 0.1℃ for those below 50℃, and ± 2℃ for temperatures above 100℃. Phase changes observed during the analyses were the quasi-eutectic, or initial ice-melting temperatures (Te), carbonic solid melting temperature (Tm CO_2), final ice melting temperature (Tm ice), clathrate melting temperature (Tm CO_2-clathrate), CO_2 homogenization temperature (Th CO_2), and final liquid–vapor homogenization temperature (Th). During the analyses, the samples were cooled or heated quickly for the first cycle to observe the approximate temperatures where the phase changes occur. Then, the procedure was repeated with a slower heating rate as the temperature of the phase change was approached.

4.2. Fluid inclusion and mineral LA-ICP-MS analyses

Fluid inclusion analyses with Laser Ablation Inductively Coupled Plasma Mass Spectrometry (LA-ICP-MS) were performed at the Single Inclusion LA-ICP-MS Laboratory at Nanjing University using a 193-nm ArF Excimer Laser System (GeolasHD from Coherent) coupled with a Perkin Elmer 350 × quadrupole ICP-MS. The instrumental and data acquisition parameters used for analyzing quartz-hosted FIs are detailed in Pan et al. (2019). The isotopes measured in this study include ^{7}Li, ^{9}Be, ^{11}B, ^{23}Na, ^{24}Mg, ^{27}Al, ^{29}Si, ^{31}P, ^{34}S, ^{35}Cl, ^{39}K, ^{44}Ca, ^{45}Sc, ^{47}Ti, ^{55}Mn, ^{57}Fe, ^{65}Cu, ^{66}Zn, ^{69}Ga, ^{72}Ge, ^{75}As, ^{79}Br, ^{85}Rb, ^{88}Sr, ^{89}Y, ^{90}Zr, ^{93}Nb, ^{95}Mo, ^{118}Sn, ^{121}Sb, ^{133}Cs, ^{137}Ba, ^{139}La, ^{140}Ce, ^{141}Pr, ^{146}Nd, ^{147}Sm, ^{153}Eu, ^{157}Gd, ^{159}Tb, ^{163}Dy, ^{165}Ho, ^{166}Er, ^{169}Tm, ^{172}Yb, ^{178}Hf, ^{181}Ta, ^{182}W, ^{205}Tl, ^{208}Pb, ^{209}Bi, ^{232}Th, and ^{238}U, although, the concentrations of many isotopes were below the lower limit of detection (LOD) and are not illustrated in the result. The NIST610 reference material was used as external standard and the Na concentration of FIs as internal standard. The Na concentration of the FIs was calculated from microthermometric data by using experimentally known T-X relations for FIs and empirical mass and charge balance algorithms (Heinrich et al., 2003; Allan et al., 2005). The absolute concentrations of each element were calculated by multiplying the measured ratios of these elements to Na with the Na concentration obtained from FI salinity. The reduction of LA-ICP-MS data was completed with the SILLS software (Guillong et al., 2008). Major cations of Na, Li and K in the FIs of this study were introduced into the salt correction. The 3σ of the background intensities were used to calculate the detection limits of all measured elements (Pettke et al., 2012). Based on the LA-ICP-MS data of the analyzed fluid inclusions, the average elemental concentrations with ±1σ uncertainties for each FIA were also calculated.

Trace element composition of quartz was quantified using the matrix signals when analyzing the quartz-hosted FI with LA-ICP-MS. A 100 wt% of SiO_2 was taken as the internal standard to determine the element concentrations in quartz. Data acquisition parameters and isotopes measured during the analyses of spodumene were consistent with that for quartz ablation. The NIST610 also served as the external standard and ^{27}Al was used as the internal standard based on the spodumene stoichiometry of $LiAlSi_2O_6$.

4.3. SEM-EDS analyses

Scanning electron microscope (SEM) imaging and energy dispersive spectroscopic (EDS) analyses were performed on thin sections of the pegmatite dike from both inner and outer zones to qualitatively determine the major and accessory mineral compositions. The analyses were carried out at the Southern University of Science and Technology, China using a Zeiss sigma 300 field emission scanning electron microscope (FE-SEM) fitted with a Bruker e-FlashFS EBSD detector and an XFlash 6–60 EDS-SDD detector. The thin sections were carbon-coated before analysis. EDS analyses were collected for 50 s at an accelerating voltage of 15 keV, 100 μA beam current and a working distance of 8.3 mm.

5. Results

5.1. Fluid inclusion petrography and microthermometry

All fluid inclusions investigated in this study were hosted in quartz and spodumene crystals from the Lijiagou Li-mineralized pegmatite dike. Three types of FIs were recognized at room temperature: 1) aqueous (±carbonic) liquid–vapor (L-V); 2) carbonic monophase or liquid–vapor (L, V, L-V); and 3) crystal-bearing aqueous (±carbonic) liquid–vapor-solid (L-V-S). Fluid inclusions in the samples are either isolated or clustered without exhibiting clearly determined origin; are of pseudo-secondary origin growing along short trails within the crystal; or are of secondary origin occurring along healed fractures crosscutting the grain boundaries. Only a few FIs seems to be aligned along growth zones, which are likely to be of primary origin. However, it cannot be exactly excluded that they occur along the pseudo-secondary trail as the growth zone in this quartz was not clearly present. A limited number of FIs appear to exhibit alignment along growth zones, which are presumably of primary origin. Nevertheless, it is important to acknowledge that the possibility of their occurrence along pseudo-secondary trails cannot be definitively ruled out, given the absence of a clearly discernible growth zone in the quartz sample under consideration. The well-defined fluid inclusion assemblages (FIA), especially those that were likely entrapped during the pegmatite crystallization are the main focus of this study. Sometimes, FIs of pseudo-secondary or primary origin are disguised by well-developed FIs along secondary healed fractures, for instance, in quartz samples from the inner zone. Fluid inclusions from these samples were excluded from further compositional study.

The result of fluid inclusion microthermometry is shown in Table 1. Initial ice-melting or eutectic temperature (Te) was difficult to observe in inclusions in quartz, whereas it was recognized in some FIs hosted in spodumene. The salinity of the fluid inclusions (wt.% of NaCl equivalent) were calculated from the final ice melting temperature (Tm ice) using the equation of Bodnar (1993) for aqueous fluid inclusions without the presence of significant amount of CO_2. The salinity of

Table 1
Results of the microthermometric analyses of fluid inclusions in quartz and spodumene from the pegmatite dike.

Host mineral	Location	FI type	FIA code & FI number	Paragenesis	Te (°C)	Tm CO_2-clathrate (°C)	Tm ice (°C)	Th CO_2 (°C)	Th-final (°C)	Salinity (wt. %)
Qz	outer zone	aqueous L-V, type 1b	FIA-1, (2)	Pseudo-secondary	/	/	−2.5 ~ -2.4	/	198 ~ 202	4.1
Qz	outer zone	aqueous L-V, type 1b	FIA-2, (2)	Pseudo-secondary	/	/	−2.3 ~ -2.4	/	219 ~ 222	4.0
Qz	outer zone	aqueous-carbonic L-V, type 1a	FIA-9, (3)	Pseudo-secondary	/	7.2 ~ 7.3	/	/	224 ~ 226	5.4
Qz	outer zone	aqueous L-V, type 1b	FIA-11, (3)	Secondary	/	/	−10.5 ~ -10.7	/	180 ~ 190	14.6
Qz	outer zone	aqueous-carbonic L-V, type 1a	FIA-12, (2)	Pseudo-secondary	/	6.7 ~ 6.8	/	/	/	6.4
Qz	outer zone	aqueous-carbonic L-V, type 1c	FIA-14, (2)	Secondary	/	9.9	/	23.1 ~ 23.5	/	0.2
Qz	outer zone	L_{CO2}, type 2a	FIA-4, (4)	Primary	/	/	/	2.2 ~ 17.0	/	/
Qz	outer zone	L_{CO2}, type 2a	FIA-5, (5)	Primary	/	/	/	−5.0 ~ -1.0	/	/
Qz	outer zone	L_{CO2}, type 2a	FIA-6, (2)	Pseudo-secondary	/	/	/	−19.9 ~ -14	/	/
Qz	outer zone	L_{CO2}, type 2a	FIA-15, (6)	Pseudo-secondary	/	/	/	−3.0 ~ 6.0	/	/
Qz	outer zone	V_{CO2}, type 2b	FIA-7, (3)	Secondary	/	/	/	3.4 ~ 13.7	/	/
Qz	outer zone	L_{CO2}-V_{CO2}, type 2b	FIA-8, (3)	Secondary	/	/	/	25.0 ~ 30.0	/	/
Spd	inner zone	aqueous L-V, type 1b	FIA-10, (5)	Primary	−66.7	/	−2.7 ~ -6.0	/	190 ~ 280	/
Spd	inner zone	aqueous-carbonic L-V, type 1a	FIA-13, (2)	Primary	/	−1.0 ~ 0.5	/	21.5 ~ 24.5	314 ~ 317	15.9
Spd	inner zone	L_{CO2}, type 2a	FIA-3, (6)	Primary	/	/	/	7.5 ~ 14.2	/	/
Spd	inner zone	L-V-S, type 3	FIA-16, (2)	Primary	/	9.9	/	/	295 ~ 328*	/

*For FIA-16, the T_h-final of 295 ~ 328 °C here denotes the vapor disappearance temperature, while the solid phase was not dissolved even up to 500 °C.

aqueous-carbonic fluid inclusions was calculated from the final melting temperature of CO_2 clathrate (Tm CO_2-clathrate) using the algorithm of Steele-MacInnis (2018).

5.1.1. *Type 1 fluid inclusions*

Type 1 or aqueous (±carbonic) liquid–vapor (L-V) fluid inclusions are quite common in crystal samples from both the inner and the outer zones of the pegmatite dike. Many of these inclusions grew along secondary healed fractures (Fig. 5a), especially in quartz in the inner zone. However, some FIs were observed as clusters along pseudo-secondary trails (Fig. 5b) and were interpreted to be trapped approximately at the same time as the formation of the pegmatite dike, therefore, these inclusions were the main focus of further analyses. These FIs are generally small (mostly 5–25 μm in diameter) with ovoid, elongated or irregular shape. Based on which phase (liquid or vapor) the type 1 fluid inclusions being homogenized to, they are categorized into two distinct classes; one for those being homogenized into the liquid phase (type 1a & type 1b; Fig. 5a, b), while the other being homogenized into the vapor phase (type 1c; Fig. 5d, e). In general, solid CO_2 or CO_2 clathrate was likely to be observed in type 1a inclusions (Fig. 5b); for those without detectable CO_2 were denoted as type 1b (Fig. 5a). The salinities of type 1a inclusions were estimated with the measured CO_2-clathrate melting temperatures, and those for type 1b fluid inclusions were calculated based on the measured ice-melting temperatures.

Type 1a and 1b inclusions account for ~ 70–80% of the type 1 population in quartz samples from the outer zone of the pegmatite dike, and display a vapor volume proportion of 4–25 vol%. Type 1a and 1b inclusions are also more commonly observed in spodumene from the inner zone (Fig. 5c) where type 1c inclusions are rare. Fluid inclusions in spodumene occur along the c-axis of the crystal, generally display elongated negative crystal shapes, which are possibly the primary fluid inclusions. Also, these type 1a and 1b fluid inclusions in spodumene are characterized by a vapor phase of 4–20 vol%.

Type 1c inclusions are generally 5–30 μm in size, have oval or irregular shape, and commonly occur along secondary healed fractures and, in some cases, coexist with monophase vapor CO_2 inclusions (i.e., type 2b inclusion, Fig. 5d, e). A small proportion of this type is isolated and undetermined in origin. Type 1c inclusions are less common than the type 1a and type 1b FIs and are mainly observed in quartz. They display low salinity (0.2 wt% NaCl eq.), a vapor phase above 65 vol%, and homogenize to the vapor phase. However, the exact homogenization temperature for this type of FIs is generally difficult to observe and FIs sometimes easily decrepitate before homogenization during the heating process.

The initial ice melting temperature observed in one FIA of type 1b in spodumene was around −67℃. This is significantly lower than the eutectic temperature of the NaCl-H_2O system (-21.2℃, Davis et al., 1990) and NaCl-KCl-H_2O system (–22℃, Sterner et al., 1988), and is much closer to the eutectic temperature of LiCl-H_2O system (-75.5℃, Conde, 2004). It indicates that LiCl is probably included in the fluids, which is confirmed by the results of LA-ICP-MS analyses of type 1a and 1b FIs where high concentrations of Li were measured in the fluids. The final homogenization temperature of type 1a and 1b FIs is between 182℃ and 317℃. Most of the primary or pseudo-secondary type 1a and 1b inclusions underwent final ice-melting temperature in the range between −2.3℃ and −6℃, or CO_2 clathrate melting temperature from −1.0℃ to 7.3℃, corresponding to a salinity between 4 and 15.9 wt% of NaCl eq. for the fluids. However, the final homogenization temperatures for FIA-10 inclusions in spodumene vary widely (190-280℃, Table 1) relative to other FIAs, indicating that they might underwent post-entrapment modification, therefore, these inclusions were excluded from further study.

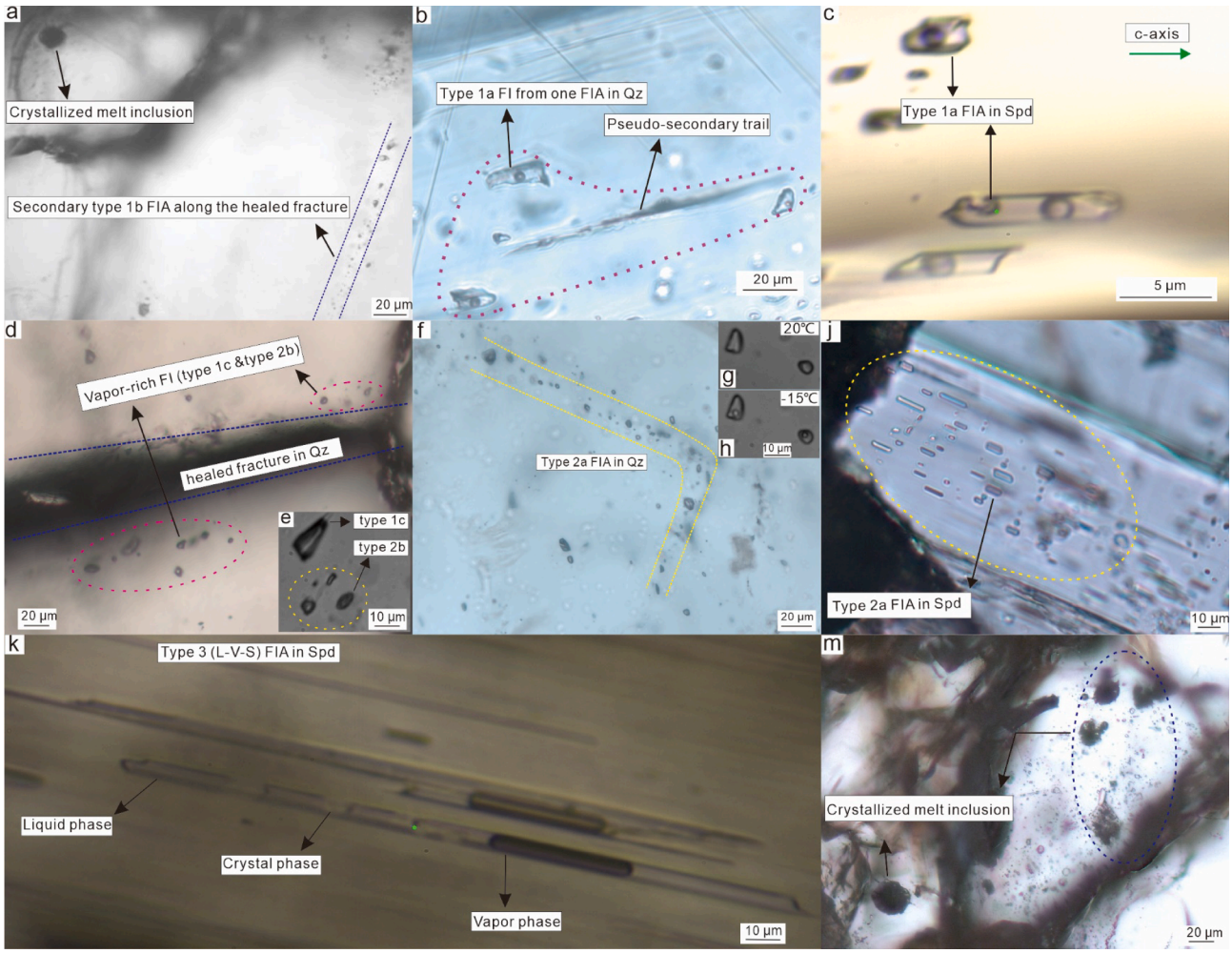

Fig. 5. Microphotographs of fluid inclusions in quartz and spodumene. (a) Secondary FIs occurring along a healed fracture in quartz from the outer zone, and an isolated crystallized melt inclusion. (b) Type 1a FIs appearing along pseudo-secondary trail in quartz from the outer zone. (c) Type 1a FIs hosted in spodumene from the inner zone displaying negative crystal shape, elongated parallel to the c-axis of the spodumene. (d) Vapor-rich fluid inclusions of type 1c and 2b occurring along healed fractures in quartz from the outer zone, the fracture has crosscut the quartz crystal and is denoted by the blue dashed line, and (e) a closer look at these inclusions. (f) Type 2a inclusions present along growth zone or pseudo-secondary trail as an assemblage in quartz from the outer zone, and have been defined by the yellow dashed line. Also, representative inclusions at 20 ℃ and −15℃ are shown in (g) and (h), respectively. (j) Type 2a inclusions in spodumene with negative spodumene crystal shape. (k) Two type 3 FIs in spodumene with elongated shape, containing liquid, vapor, and solid phases. (m) Assemblage of melt inclusions hosted in quartz from the outer zone. See text for detailed description. (For interpretation of the references to colour in this figure legend, the reader is referred to the web version of this article.)

5.1.2. *Type 2 fluid inclusions*

Type 2 FIs are carbonic inclusions containing almost pure CO_2 with the possibility of small amount of aqueous phase wetting the inclusion wall. They can be subdivided into type 2a (Fig. 5f), which homogenizes to liquid CO_2, and type 2b which homogenizes to vapor CO_2 (Fig. 5e). Type 2 FIs are commonly observed in both quartz from the outer zone and spodumene from the inner zone. They have round, oval or irregular shapes in quartz and are mainly elongated in spodumene with typically 5–20 μm across. In many cases, the type 2 inclusions are monophase, either liquid (Fig. 5g, h) or vapor (Fig. 5e) at room temperature (~25℃). Both type 2a and type 2b inclusions were observed in quartz from the outer zone with the predominance of type 2a FIs (~60–80%). Type 2a inclusions in quartz typically occur along pseudo-secondary trails, growth zones or as clusters with undetermined origin. Type 2a FIs of secondary origin (i.e., along fractures crosscutting the crystals) have not been found in the samples. Type 2b inclusions are mainly present in quartz from the outer zone and mostly occur either along secondary trails or clusters of undetermined origin, with few clearly showing primary origin. In spodumene from the inner zone, type 2a inclusions commonly occur with negative crystal shape along the c-axis (Fig. 5j) but type 2b FIs are extremely rare.

The final melting temperature of a solid phase observed at −56.8℃ to −56.9℃ in type 2 FIs indicates the presence of CO_2 (triple point of CO_2 is at −56.6℃, 0.5 MPa) and possibly traces of other volatiles. The homogenization temperatures of primary or pseudo-secondary type 2a FIs range from −19.9℃ to 17℃, which correspond to CO_2 density between 1.03 g/cm^3 and 0.80 g/cm^3. The type 2b inclusions, which are mainly secondary in quartz, show a broad homogenization temperature range from 3.4℃ to 30℃ corresponding to CO_2 density of 0.11–0.34 g/cm^3.

5.1.3. *Type 3 fluid inclusions*

The three-phase (L-V-S) type 3 FIs are mainly observed in spodumene from the inner zone of the pegmatite dike. The FIs are 5 μm to 120 μm in length and have an elongated negative spodumene crystal shape (Fig. 5k). The composition of the liquid and vapor phase is mainly aqueous ± carbonic, as CO_2 can be recognized in some but not all FIs with microthermometry. Type 3 inclusions analyzed in one FIA in spodumene show CO_2 clathrate melting temperature ~ 9.9℃, while the vapor homogenization temperature varies widely between 295℃ and

328℃ which might be the result of post-entrapment modification. The solid phases in the FIs were not dissolved or melted even after heating the inclusions up to 500℃. Also, as similar crystal-bearing inclusions were not observed in the quartz intergrown with spodumene, these FIs in spodumene might have underwent post-entrapment modification.

Though type 3 FIs were not analyzed further, they are indicative of the presence of aqueous ± carbonic fluid during spodumene crystallization, which might correlate with type 1 FIs trapped in quartz in the outer zone.

5.1.4. Silicate melt inclusions

Apart from the three types of FIs mentioned above, crystallized melt inclusions (MI) were also observed in quartz from the outer zone (Fig. 5a, m). These inclusions commonly display round or irregular shapes, and are relatively large (20–200 μm in length) compared to type 1 and 2 FIs in quartz. The inclusions typically would not be homogenized until up to ~ 1200-1350℃ at atmospheric pressure during microthermometry. The observed homogenization temperature is much higher than that of a general granitic melt inclusion from intrusive rocks (Yuan et al., 2021). This can be the result of either heterogeneous entrapment of melt and crystalizing mineral phase(s); water loss from the inclusion; or the low confining pressure (~1 bar) during the homogenization experiment compared to the pressure where the MI was originally entrapped. This type of inclusion is indicative of the presence of silicate melt in the pegmatitic system in addition to the aqueous and carbonic fluids during pegmatite formation.

5.2. Element concentrations in fluid inclusions

Representative FIs of both type 1 and type 2 were analyzed with LA-ICP-MS to obtain the major and trace element composition of the fluids. However, only the quartz-hosted type 1a and 1b FIs provided clear signal, whereas clear FIs signals were seldom present when analyzing the type 1c and type 2 inclusions. In the latter two types, a single Na peak was present occasionally which can be the result of too low concentrations of other elements in these inclusions. Additionally, no clear FIs signals in spodumene were obtained. The elemental concentrations of individual FIs and the average composition of each FIAs are presented in Table 2. According to the results, the element concentrations of the inclusions within each individual FIAs are consistent and the compositions for all type 1a and 1b inclusions analyzed are basically uniform. Specifically, Li, Na, K and Cs concentrations were steadily yielded in all inclusions, while the concentrations of other elements were either fully or partly below the detection limit. Li and Na are the most abundant two cations in these FIs with the concentration of thousands of ppm (3000–6100 ppm Li; 3500–9400 ppm Na), and the ratios of Li to Na ranging from 0.5 to 1.3. Other cations present in the FIs above the LOD include K (300–1200 ppm, mostly < 1000 ppm), Cs (10–540 ppm, mostly > 50 ppm), Sr (10–520 ppm), Rb (10–50 ppm), and Ba (30–120 ppm). Rb and Sr concentrations were obtained in all but two analyzed FIs and Ba concentrations were obtained in nearly half of the inclusions. All additional elements analyzed were below the LOD and are not reported in the results.

5.3. Element concentrations in quartz and spodumene

The trace element concentration of quartz from the outer zone was obtained from analyzing the quartz hosts of the FIs with LA-ICP-MS. The results are presented in Table 3. Concentrations of Al, Li, Ge and Na were obtained for all analytical spots in quartz. Each of these elements show a narrow range of concentrations: 210–328 ppm Al, 45–66 ppm Li, 5–10 ppm Ge, and 2–5 ppm Na. The concentrations of other elements in quartz were below the LOD.

The spodumene from the inner zone was also analyzed with LA-ICP-MS. The absolute concentration of elements was obtained using the ratios of each cation to Al abundance and the calculated Al concentration according to the stoichiometry of spodumene. This calculation was completed by first normalizing the mass of all major oxides (>0.01 wt%) of the cations to 100 wt%, then taking the individual proportions of each

Table 3
Results of LA-ICP-MS analyses of quartz from the outer zone of the pegmatite dike.

Spot No.	Li	Na	Al	Sc	Ge	Fe	Ca
	μg/g	μg/g	μg/g	μg/g	μg/g	μg/g	μg/g
1a-1(A)	47	3	210	1	5	<32	<226
1a-2(A)	51	3	235	1	7	<8	<53
1a-2(B)	55	5	254	1	7	<31	<213
1a-3(A)	51	3	246	1	6	10	<80
1a-4(A)	62	3	247	1	7	<9	244
1a-4(B)	66	2	328	<1	8	<22	169
1a-4(C)	60	2	285	<1	8	<11	<68
1a-4(D)	63	3	257	1	7	<4	277
1a-4(E)	50	2	228	1	7	<5	124
1a-5(A)	45	2	252	<1	10	<42	<403

Table 2
Results of fluid inclusion LA-ICP-MS analyses in quartz from the outer zone of the pegmatite dike.

FI type	FIA & analyzed numbers	Salinity	FI No.	Li	Na	K	Rb	Sr	Cs	Ba	Li/(K + Na)	K/Na	Rb/Na	Cs/Na	Cs/Rb
		wt.%		μg/g	μg/g	μg/g	μg/g	μg/g	μg/g	μg/g					
Type 1a	1a-1, (4)	6.4	1	6107	4660	483	30	244	256	58	1.187	0.104	0.0064	0.055	8.53
			2	6099	4644	554	45	213	399	<50	1.173	0.119	0.0097	0.086	8.87
			3	6027	4862	590	26	382	254	123	1.105	0.121	0.0053	0.052	9.77
			4	5870	5506	381	48	239	325	67	0.997	0.069	0.0087	0.059	6.77
			avg.	6026	4918	502	37	270	309	83	1.116	0.103	0.0075	0.063	8.49
			stdev.	110	404	92	11	76	69	35	0.087	0.024	0.0020	0.016	1.26
	1a-2, (2)	6.4	1	5344	7002	796	32	306	304	76	0.685	0.114	0.0046	0.043	9.50
			2	5308	6911	1156	38	271	245	<109	0.658	0.167	0.0055	0.035	6.45
			avg.	5326	6957	976	35	289	274	76	0.672	0.140	0.0050	0.039	7.97
			stdev.	25	64	255	4	25	42	–	0.019	0.037	0.0006	0.006	2.16
	1a-3, (1)	6.4	1	4646	9204	988	42	515	540	<88	0.456	0.107	0.0046	0.059	12.86
Type 1b	1a-4, (2)	4	1	3077	5219	547	<15	<13	13	<141	0.534	0.105	–	0.002	–
			2	3300	4657	521	<28	<32	28	<62	0.637	0.112	–	0.006	–
			avg.	3188	4938	534	–	–	21	–	0.585	0.108	–	0.004	–
			stdev.	158	397	18	–	–	11	–	0.073	0.005	–	0.003	–
	1a-5, (2)	4	1	3636	3493	333	15	18	79	<48	0.950	0.095	0.0043	0.023	5.27
			2	3542	4001	344	19	17	61	<78	0.815	0.086	0.0047	0.015	3.21
			avg.	3589	3747	339	17	17	70	–	0.883	0.091	0.0045	0.019	4.24
			stdev.	66	359	8	3	1	13	–	0.095	0.006	0.0003	0.006	1.46

* "-" denotes that the value was unable to be obtained by calculation.

oxide components. The concentrations of main components of spodumene (Li_2O, Al_2O_3, SiO_2) are reported in weight percent (wt.%) and the concentrations of other minor or trace elements are shown in parts per million (ppm) in Table 4. The mole ratios of Li, Al and Si were close to the stoichiometry of spodumene ($LiAlSi_2O_6$). The cations of Na, Mn, Fe, Mg, Ti, Ga, Nb, Sn, and Ta were also present showing a narrow concentration range. The most abundant trace element in spodumene is Fe, displaying a higher concentration (1512–1663 ppm) than the total concentration of other trace elements (334–512 ppm Na, 244–520 ppm Mn, 66–137 ppm Ti, 24–27 ppm Ga, 7–11 ppm Mg, 8–17 ppm Sn, 1–8 ppm Nb, 0–2 ppm Ta).

6. Discussion

6.1. The composition and origin of the pegmatitic aqueous ± carbonic fluids

Melt inclusions were present in quartz from the outer zone suggesting the presence of silicate melt in the pegmatite system. Besides that, it is evident that both aqueous ± carbonic fluids and carbonic fluids were present in the system during the pegmatite evolution which is represented by the primary or pseudo-secondary type 1 and type 2 FIs. As noted earlier, the type 3 (L-V-S) inclusions hosted in spodumene possibly underwent post-entrapment modification and mainly reflect the presence of aqueous-carbonic fluid in the ore-forming system. Only the type 1a and 1b FIs provided clear fluid inclusion signals and consistent elemental composition data during the single fluid inclusion LA-ICP-MS analyses, whereas concentrations in type 1c and type 2 FIs were below the detection limit. Accordingly, the low density aqueous-carbonic fluids and the carbonic fluids in this system did not carry significant Li during pegmatite formation.

The results of type 1a and 1b inclusion LA-ICP-MS analyses are shown in Table 2. The elements of Na, Li, K, Rb, Sr, and Cs were detected in all or most FIs and Ba was detected in nearly half of the FIs. It has been reported that K, Rb and Cs are variably enriched in magmatic-hydrothermal fluids associated with intrusive felsic rocks (Heinrich et al., 1999; Landtwing et al., 2010). The abundances of K and Rb relative to Na are usually used to distinguish the fluids with magmatic-hydrothermal origin from other sources (Samson et al., 2008). According to the K/Na-Rb/Na plot shown in Fig. 6a, the inclusions analyzed consistently lie within the range of magmatic-hydrothermal origin. The highly incompatible Cs is indicative of the evolution degree of the magmatic-hydrothermal system, since the increasing Cs concentration in the residual melt and accompanied exsolved fluids is generally caused by magma crystallization (Audétat et al., 2008; Klemm et al., 2008). In this study, the measured Cs concentration in the FIs was variably enriched (13–540 ppm, mostly with several hundreds of parts per million), suggesting magmatic-hydrothermal fluid characteristics opposed to a sedimentary origin, taking into account that the Triassic sedimentary rocks in this region contain extremely low Cs concentrations (~2–15 ppm, Sigoyer et al., 2014). Rubidium is another incompatible alkali element, and its concentration increase in the fluid with increasing Cs concentration (Fig. 6b). This suggests that similarly to Cs, the Rb abundance in the fluids was controlled by the internal magmatic-hydrothermal evolution of the system. Furthermore, Rb and Cs are hydrothermally non-reactive and therefore largely conservative components in hydrothermal fluids, making the ratio of Cs/Rb an ideal tool to identify the fluid source (Klemm et al., 2008; Korges et al., 2018). The Cs/Rb ratios of FIs in this study lie within a narrow range from 4 to 15 (Fig. 6b) and are all above or near the dilution line suggesting that meteoric water was barely involved during the pegmatite formation (Pan et al., 2019). The obtained Cs/Rb values are similar to that reported in the fluids in the Yaogangxian W deposit (Cs/Rb: 4–20) which was interpreted to have a single magmatic fluid source (Pan et al., 2019). Accordingly, the fluids represented by the FIs in this study should predominately originated from the pegmatitic system at the magmatic-hydrothermal transition stage. Lithium is enriched in the pegmatitic aqueous fluids represented by the type 1a and 1b fluid inclusions. Furthermore, it shows generally increasing concentrations with increasing Cs concentrations, implied by the approximately positive correlation between Li and Cs relative to the total abundance of Na + K (Fig. 7). Note should be taken to the fact that lithium shows high concentrations even at relatively low Cs concentrations in the fluids. This indicates that Li is enriched at the early magmatic-hydrothermal transition stage of the pegmatitic system and it is further concentrated as the magma crystallization proceeds.

Additionally, it has been reported that magmatic and metasomatic spodumene show different trace elemental abundances, especially for Fe and Mn (Brennan et al., 2021). Secondary metasomatic spodumene growing from hydrothermal fluids and as a product of petalite breakdown reaction contains low abundance of Mn and Fe (Mn $\leq$ 200 ppm, Fe $\leq$ 200 ppm), while concentrations of these two elements in primary magmatic spodumene growing at magmatic to hydrothermal transition are generally higher (Mn $\geq$ 350 ppm, Fe $\geq$ 2000 ppm) (Brennan et al., 2021). According to the result of spodumene LA-ICP-MS analyses shown in Table 4, the concentrations of Mn and Fe in spodumene (Mn: 244–520 ppm; Fe: 1512–1663 ppm) suggest that the spodumene in this study was more likely to form at the magmatic to hydrothermal transition stage rather than at the metasomatic stage. The absence of petalite or the intergrowth of spodumene + quartz ± petalite in the Lijiagou albite-spodumene pegmatite also suggests that spodumene was unlikely to form by petalite metasomatism.

6.2. The implication for Li mineralization from fluids and quartz composition

In general, common pegmatitic minerals from Li-mineralized pegmatitic systems are expected to contain elevated concentration of Li. Particularly, the Li concentration in pegmatitic quartz is considered as a useful geochemical indicator to imply the Li enrichment degree and Li mineralization potential of the pegmatitic system (Beurlen et al., 2014; Maneta & Baker, 2019). Maneta & Baker (2019) proposed that in the Moblan pegmatite from Quebec, the high Li concentrations in quartz (>30 ppm) indicate the crystallization of Li-aluminosilicate mineral in the pegmatite system. Likewise, Beurlen et al. (2014) demonstrated that Li concentrations exceeding 50 ppm in quartz is a reliable indicator for identifying spodumene-rich pegmatites. Quartz samples analyzed from the outer zone of the Lijiagou albite-spodumene pegmatite show uniformly high incorporation of Li in quartz with an average concentration of 56 ± 7 (1σ) ppm (Table 3). This can be indicative of the Li mineralization potential of the pegmatitic system in this area.

In type 1a and 1b inclusions, Na, Li and K are the three most

Table 4
Results of LA-ICP-MS analyses of spodumene from the inner zone of the pegmatite dike.

Spot No.	Li_2O	Al_2O_3	SiO_2	Na	Mn	Fe	Mg	Ti	Ga	Nb	Sn	Ta
	wt.%	wt.%	wt.%	μg/g	μg/g	μg/g	μg/g	μg/g	μg/g	μg/g	μg/g	μg/g
Spd-1	7.26	28.06	64.37	512	255	1634	11	137	27	8	8	2
Spd-3	6.99	27.73	64.99	480	244	1512	8	124	25	6	11	2
Spd-4	7.12	27.96	64.62	334	481	1522	7	66	26	1	12	<1
Spd-5	7.38	28.48	63.81	345	520	1663	8	89	24	1	17	<1

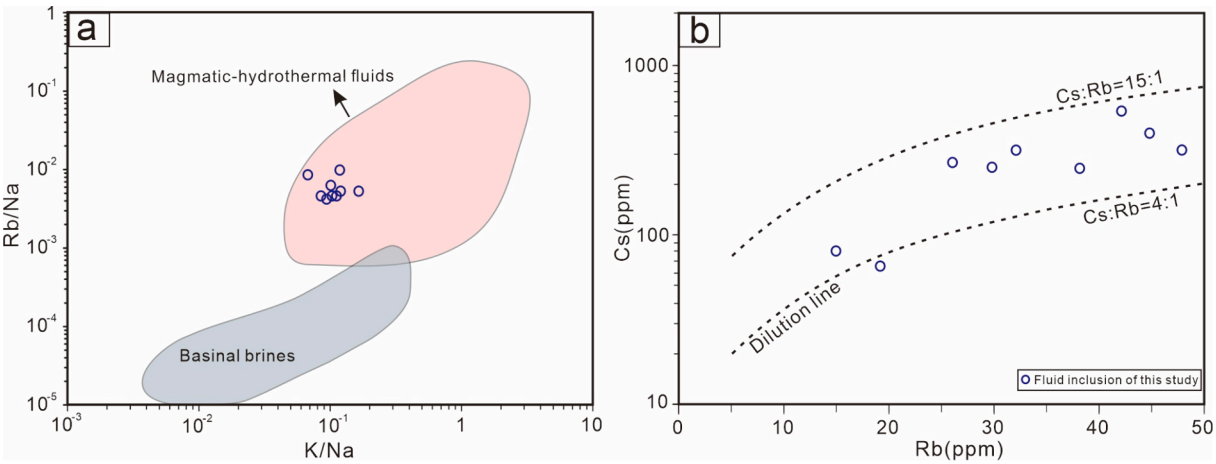

Fig. 6. Diagrams of selected element concentrations and concentration ratios of type 1a and 1b pseudo-secondary fluid inclusions for identifying the fluids source. (a) The pink and grey regions represent Rb/Na and K/Na ratios of fluids of magmatic-hydrothermal and basinal brine origin, respectively, according to Pan et al. (2019). (b) The Cs and Rb concentrations of FIs indicate that meteoric water was barely involved in the studied pegmatitic system. (For interpretation of the references to colour in this figure legend, the reader is referred to the web version of this article.)

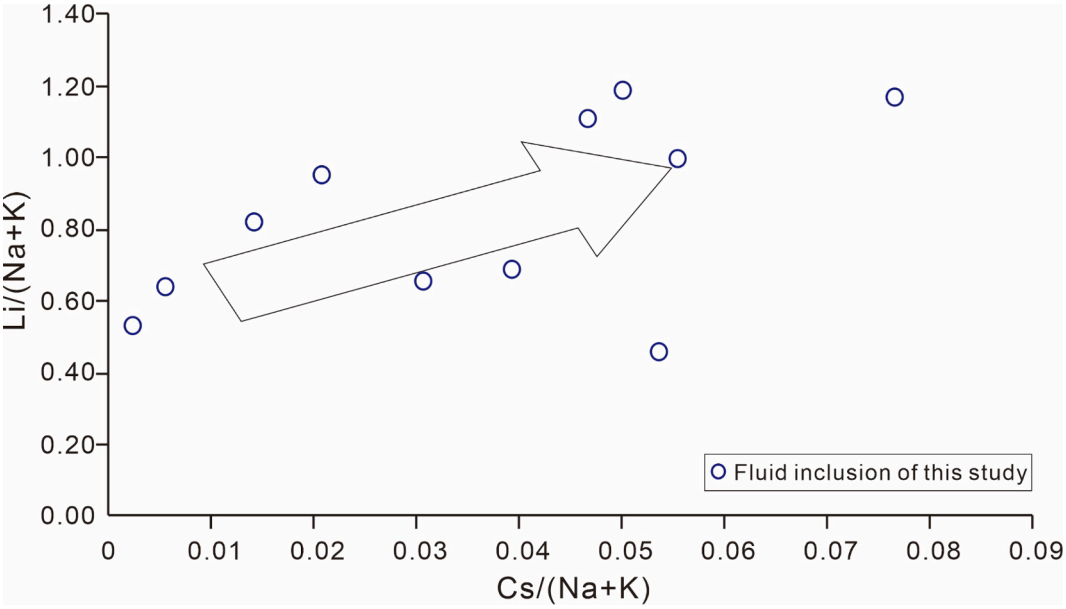

Fig. 7. The diagram of Li/(Na + K) versus Cs/(Na + K) shows the increasing relative abundance of Li in the fluids with increasing relative Cs abundance.

abundant cations accounting for>90% of the total concentrations of all cations. Particularly, Na and Li predominate the cations abundance in the system as shown by the Na-Li-K ternary diagram (Fig. 8a) and by the ratios of Li to (Na + K) ranging from 0.4:1 to 1.2:1 (Fig. 8b). This fluid composition is somewhat different from the general magmatic-hydrothermal fluids related to intrusive igneous rocks, especially in comparison to those associated with non-ferrous metal mineralization (e.g., Cu, Mo, W, Sn) where Na and K are the predominant cations rather than Li and Na (Audétat, 2019). Fig. 9 summarizes the elemental compositions of Na, Li, and K in fluids from both lithium-cesium-tantalum (LCT) and niobium-yttrium-fluorine (NYF) pegmatitic systems form single fluid inclusion LA-ICP-MS analyses (Van Daele et al., 2018; Gammel & Nabelek, 2016; Richter, 2015; Berni et al., 2020; Michallik et al., 2021). Although the relative Li abundance in both the LCT and NYF systems is widely distributed, its upper limit in the LCT system (Li/Na: 0.01–1, Li/K: 0.01—10) is higher than in the NYF system (Li/Na: 0.001–0.1, Li/K: 0.01–1). This implies that Li could become more enriched in the pegmatitic fluids (silicate melt and aqueous ± carbonic fluids) during the pegmatite evolution in LCT systems when compared to NYF pegmatitic fluids. The relative Li concentrations of fluids in the albite-spodumene pegmatite of this study lie within the uppermost range of Li/Na and Li/K of fluids in LCT systems (Fig. 9). This shows that Li concentration in the aqueous ± carbonic fluids could be as enriched as Na in the Li-mineralized pegmatitic system, and it is also indicative of the high Li abundance in the pegmatitic melt from which the aqueous ± carbonic fluids were exsolved. Hence, similarly to the elevated incorporation of Li in quartz, the high enrichment degree of Li in the pegmatitic aqueous fluid at the magmatic-hydrothermal transition stage suggests high Li abundance in the pegmatitic melt and could be indicative of the Li mineralization potential in the pegmatitic system.

7. Conclusion

Different types of fluid inclusions were identified in quartz and spodumene from the Lijiagou albite-spodumene pegmatite including primary, pseudo-secondary and secondary fluid inclusions of aqueous ±

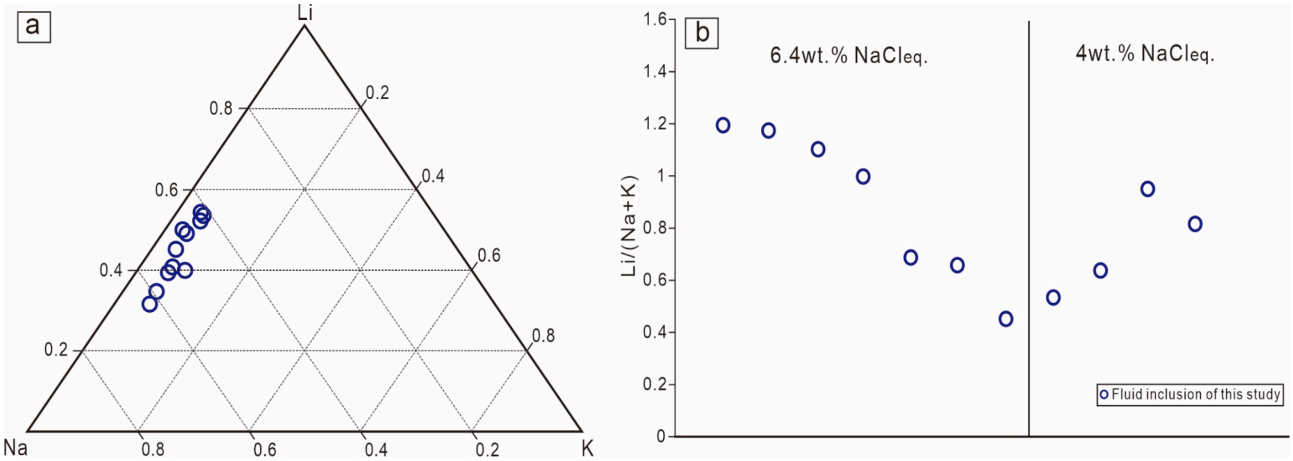

Fig. 8. (a) Ternary plot of the three most abundant cations (Na, Li, K) in the type 1a and 1b fluid inclusions showing that Li and Na predominate the cations in the fluids. (b) The diagram depicts the concentration of Li relative to Na + K in the same fluid inclusions indicating high concentrations of Li in the aqueous ± carbonic fluids.

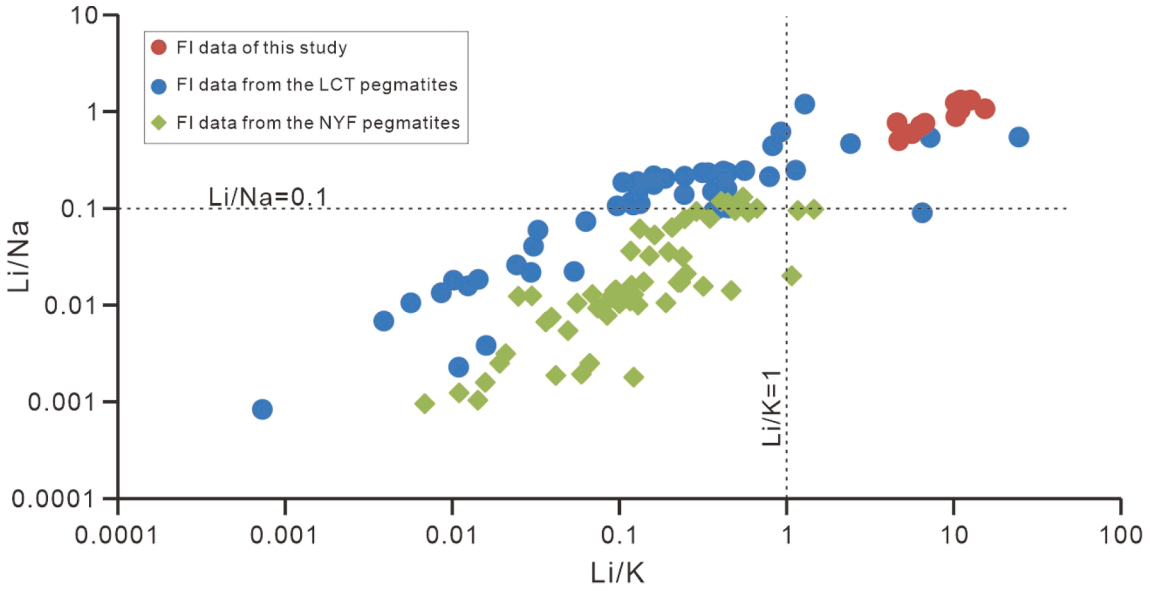

Fig. 9. The diagram shows Li/Na versus Li/K ratios in the fluid inclusions based on the results of single fluid inclusion LA-ICP-MS analyses of this study and previous research from both lithium-cesium-tantalum (LCT) and niobium-yttrium-fluorine (NYF) pegmatitic systems (Van Daele et al., 2018; Gammel et al., 2016; Richter et al., 2015; Berni et al., 2020; Michallike et al., 2021).

carbonic and carbonic compositions in addition to silicate melt inclusions. This suggests that the albite-spodumene pegmatite underwent both magmatic-hydrothermal transition and post-crystallization hydrothermal processes during its formation and evolution. The result of fluid inclusion LA-ICP-MS analyses shows that the aqueous ± carbonic fluid represented by the pseudo-secondary type 1a and 1b inclusions was the major fluid phase carrying Li in the pegmatitic system. The compositional characteristics of the fluid indicate that it originated from a magmatic-hydrothermal source at the magmatic-hydrothermal transition stage. This is consistent with the composition of spodumene in the pegmatite dike showing magmatic trace element compositional characteristics rather than metasomatic characteristics. The pegmatitic fluids obtained are characterized by the predominance of Na and Li cations. The relative abundance of Li to Na and K lies within the uppermost range of those reported from lithium-cesium-tantalum pegmatite systems. The high degree of Li enrichment in the pegmatitic aqueous fluid occurred at the magmatic and hydrothermal transition stage and can be indicative of the Li mineralization potential in pegmatitic system. This coincides with the elevated incorporation of Li in the pegmatitic quartz from the outer zone of the dike which also indicates the enrichment of Li in pegmatitic system during its formation.

Declaration of Competing Interest

The authors declare that they have no known competing financial interests or personal relationships that could have appeared to influence the work reported in this paper.

Data availability

Data will be made available on request.

Acknowledgements

This work was supported by the National Natural Science Foundation of China (Grant Nos. 42030303, 41872051, 41973055, 42130109 and

42303032) and the Stable Support Plan Program of Shenzhen Natural Science Fund (Grant No. GXWD20201230110313001, Program Contract No. 20200925161932001).

References

Allan, M.M., Yardley, B.W., Forbes, L.J., Shmulovich, K.I., Banks, D.A., Shepherd, T.J., 2005. Validation of LA-ICP-MS fluid inclusion analysis with synthetic fluid inclusions. Am. Mineral. 90, 1767–1775. https://doi.org/10.2138/am.2005.1822.

Audétat, A., 2019. The metal content of magmatic-hydrothermal fluids and its relationship to mineralization potential. Econ. Geol. 114 (6), 1033–1056. https://doi.org/10.5382/econgeo.4673.

Audétat, A., Pettke, T., 2003. The magmatic-hydrothermal evolution of two barren granites: A melt and fluid inclusion study of the Rito del Medio and Canada Pinabete plutons in northern New Mexico (USA). Geochim. Cosmochim. Acta 67, 97–121. https://doi.org/10.1016/S0016-7037(02)01049-9.

Audétat, A., Pettke, T., Heinrich, C.A., Bodnar, R.J., 2008. The composition of magmatic-hydrothermal fluids in barren versus mineralized intrusions. Econ. Geol. 103, 877–908. https://doi.org/10.2113/gsecongeo.103.5.877.

Barros, R., Kaeter, D., Menuge, J.F., Skoda, R., 2020. Controls on chemical evolution and rare element enrichment in crystallising albite-spodumene pegmatite and wallrocks: Constraints from mineral chemistry. Lithos 352–353, 105289. https://doi.org/10.1016/j.lithos.2019.105289.

Berni, G.V., Wagner, T., Fusswinkel, T., 2020. From a F-rich granite to a NYF pegmatite: magmatic-hydrothermal fluid evolution of the Kymi topaz granite stock. SE Finland. Lithos 364–365, 105538. https://doi.org/10.1016/j.lithos.2020.105538.

Beurlen, H., Thomas, R., da Silva, M.R.R., Müller, A., Rhede, D., Soares, D.R., 2014. Perspectives for Li- and Ta-mineralization in the Borborema Pegmatite Province, NE Brazil: a review. J. S. Am. Earth Sci. 56, 110–127. https://doi.org/10.1016/j.jsames.2014.08.007.

Bodnar, R.J., 1993. Revised equation and table for determining the freezing point depression of H_2O-NaCl solutions. Geochim. Cosmochim. Acta 57, 683–684. https://doi.org/10.1016/0016-7037(93)90378-A.

Brennan, C., Sirbescu, M., Student, J., Hlohowskyj, S., 2021. Preliminary insights into spodumene trace element composition and speciation. In: Goldschmidt 2021 Conference Abstracts. https://doi.org/10.7185/gold2021.8090.

Burns, M.G.G., 2016. A Fluid Inclusion Study of the Little Nahanni LCT-Type Pegmatite Group, NWT Canada: Implications for the Nature and Origin of Fluids in LCT-Type Pegmatites and Pegmatite Evolution. Laurentian University, p. 104. M.Sc. Thesis.

Černý, P., Ercit, T.S., Vanstone, P.T., 1998. Mineralogy and petrology of the Tanco rare-element pegmatite deposit, Southeastern Manitoba. Field Trip Guidebook A4, Geological Association of Canada/Mineralogical Association of Canada Annual Meeting, Winnipeg, Manitoba Černý, P., Ercit, T.S., 2005. The classification of granitic pegmatites revisited. Canad. Mineral. 46, 2005–2026. https://doi.org/10.2113/gscanmin.43.6.2005.

Chen, B., Huang, C., Zhao, H., 2020. Lithium and Nd isotopic constraints on the origin of Li-poor pegmatite with implications for Li mineralization. Chem. Geol. 551, 119769 https://doi.org/10.1016/j.chemgeo.2020.119769.

Conde, M.R., 2004. Properties of aqueous solutions of lithium and calcium chlorides: formulations for use in air conditioning equipment design. Int. J. Therm. Sci. 43 (4), 367–382. https://doi.org/10.1016/j.ijthermalsci.2003.09.003.

Davis, D.W., Lowenstein, T.K., Spencer, R.J., 1990. Melting behavior of fluid inclusions in laboratory-grown halite crystals in the systems NaCl-H_2O, NaCl-KCl-H_2O, NaCl-$MgCl_2$-H_2O, and NaCl-$CaCl_2$-H_2O. Geochim. Cosmochim. Acta 54 (3), 591–601. https://doi.org/10.1016/0016-7037(90)90355-O.

Fei, G., Menuge, J.F., Li, Y., Yang, J., Deng, Y., Chen, C., et al., 2020. Petrogenesis of the Lijiagou spodumene pegmatites in Songpan-Garze Fold Belt, West Sichuan, China: Evidence from geochemistry, zircon, cassiterite and coltan U-Pb geochronology and Hf isotopic compositions. Lithos 364–365, 105555. https://doi.org/10.1016/j.lithos.2020.105555.

Fei, G., Menuge, J.F., Chen, C., Yang, Y., Deng, Y., Li, Y., Zheng, L., 2021. Evolution of pegmatite ore-forming fluid: The Lijiagou spodumene pegmatites in the Songpan-Garze Fold Belt, southwestern Sichuan province. China. Ore Geol. Rev. 139, 104441 https://doi.org/10.1016/j.oregeorev.2021.104441.

Gammel, E.M., Nabelek, P.I., 2016. Fluid inclusion examination of the transition from magmatic to hydrothermal conditions in pegmatites from San Diego County California. Am. Mineral. 101 (8), 1906–1915. https://doi.org/10.2138/am-2016-5559.

Grew, E.S., 2020. The minerals of lithium. Elements 16 (4), 235–240. https://doi.org/10.2138/gselements.16.4.235.

Gu, C., 2014. Metallogenic regularity of spodumene deposits in the closely spaced pegmatite area in the southeastern Ke' eryin pegmatite field, Sichuan Province. Contrib. Geol. Min. Resour. Res. 29 (1), 59–65.

Guillong, M., Meier, D.L., Allan, M.M., Heinrich, C.A., Yardley, B.W., 2008. Appendix A6: SILLS: A MATLAB-based program for the reduction of laser ablation ICP-MS data of homogeneous materials and inclusions. Mineral. Assoc. Canad. Short Course 40, 328–333.

Heinrich, C.A., Gunther, D., Audétat, A., Ulrich, T., Frischknecht, R., 1999. Metal fractionation between magmatic brine and vapor, determined by microanalysis of fluid inclusions. Geology 27 (8), 755–758. https://doi.org/10.1130/0091-7613(1999)027<0755:MFBMBA>2.3.CO;2.

Heinrich, C.A., Pettke, T., Halter, W.E., Aigner-Torres, M., Audétat, A., Günther, D., Horn, I., 2003. Quantitative multi-element analysis of minerals, fluid and melt inclusions by laser-ablation inductively-coupled-plasma mass-spectrometry. Geochim. Cosmochim. Acta 67 (18), 3473–3497. https://doi.org/10.1016/S0016-7037(03)00084-X.

Hulsbosch, N., Boiron, M.C., Thomas, R., Van Daele, J., Dewaele, S., Muchez, P., 2019. Evaluation of the petrogenetic significance of melt inclusions in pegmatitic schorl-dravite from graphic tourmaline-quartz assemblages: application of LA-ICP-QMS analyses and volume ratio calculations. Geochem. Cosmochim. Acta 244, 308–335. https://doi.org/10.1016/j.gca.2018.10.023.

Kaeter, D., Barros, R., Menuge, J.F., Chew, D.M., 2018. The magmatic-hydrothermal transition in rare-element pegmatites from southeast Ireland: LA-ICP-MS chemical mapping of muscovite and columbite-tantalite. Geochim. Cosmochim. Acta 240, 98–130. https://doi.org/10.1016/j.gca.2018.08.024.

Klemm, L.M., Pettke, T., Heinrich, C.A., 2008. Fluid and source magma evolution of the Questa porphyry Mo deposit, New Mexico USA. Miner. Depos. 43, 533–552. https://doi.org/10.1007/s00126-008-0181-7.

Korges, M., Weis, P., Lüders, V., Laurent, O., 2018. Depressurization and boiling of a single magmatic fluid as a mechanism for tin-tungsten deposit formation. Geology 46 (1), 75–78. https://doi.org/10.1130/G39601.1.

Landtwing, M.R., Furrer, C., Redmond, P.B., Pettke, T., Guillong, M., Heinrich, C.A., 2010. The Bingham Canyon porphyry Cu-Mo-Au deposit. III. Zoned copper-gold ore deposition by magmatic vapor expansion. Econ. Geol. 105, 91–118. https://doi.org/10.2113/gsecongeo.105.1.91.

Li, J., 2006. Mineralizing mechanism and continental geodynamics of typical pegmatite deposits in western Sichuan, China. China University of Geosciences, Beijing, pp. 1–237. Ph.D. Dissertation.

Li, J., Wang, D., Fu, X., 2006. $^{40}Ar/^{39}Ar$ ages of the Ke'eryin pegmatite type rare metal deposit, western Sichuan, and its tectonic significances. Acta Geol. Sin. 80 (6), 843–848.

Liao, Z., Zhou, Z., Zhang, H., 2019. Evidence for the geochemical characteristics of liquid immiscibility in the Keryin rare metal deposit. Acta Geol. Sichuan 39 (S1), 60–69.

Liu, C., Wang, R., Wu, F., Xie, L., Liu, X., Li, X., Yang, L., Li, X., 2020. Spodumene pegmatites from the Pusila pluton in the higher Himalaya, South Tibet: Lithium mineralization in a highly fractionated leucogranite batholith. Lithos 358–359, 105421.

London, D., 2014. A petrologic assessment of internal zonation in granitic pegmatites. Lithos 184–187, 74–104. https://doi.org/10.1016/j.lithos.2013.10.025.

Maloney, J.S., Nabelek, P.I., Sirbescu, M.L.C., Halama, R., 2008. Lithium and its isotopes in tourmaline as indicators of the crystallization process in the San Diego County pegmatites, California USA. Eur. J. Mineral. 20, 905–916. https://doi.org/10.1127/0935-1221/2008/0020-1823.

Maneta, V., Baker, D.R., 2019. The potential of lithium in alkali feldspars, quartz, and muscovite as a geochemical indicator in the exploration for lithium-rich granitic pegmatites: A case study from the spodumene-rich Moblan pegmatite, Quebec Canada. J. Geochem. Explor. 205, 106336 https://doi.org/10.1016/j.gexplo.2019.106336.

Michallik, R.M., Wagner, T., Fusswinkel, T., 2021. Late-stage fluid exsolution and fluid phase separation processes in granitic pegmatites: Insights from fluid inclusion studies of the Luumäki gem beryl pegmatite (SE Finland). Lithos 380, 105852. https://doi.org/10.1016/j.lithos.2020.105852.

Pan, J., Ni, P., Wang, R., 2019. Comparison of fluid processes in coexisting wolframite and quartz from a giant vein-type tungsten deposit, South China: insights from detailed petrography and LA-ICP-MS analysis of fluid inclusions. Am. Mineral. 104, 1092–1116. https://doi.org/10.2138/am-2019-6958.

Pettke, T., Oberli, F., Audétat, A., Guillong, M., Simon, A.C., Hanley, J.J., Klemm, L.M., 2012. Recent developments in element concentration and isotope ratio analysis of individual fluid inclusions by laser ablation single and multiple collector ICP-MS. Ore Geol. Rev. 44, 10–38. https://doi.org/10.1016/j.oregeorev.2011.11.001.

Potter, E.G., Taylor, R.P., Jones, P.C., Lalonde, A.E., Pearse, G.H.K., Rowe, R., 2009. Sokolovaite and evolved lithian micas from the eastern Moblan granitic pegmatite, Opatica subprovince, Quebec Canada. Canad. Mineral. 47, 337–349. https://doi.org/10.3749/canmin.47.2.337.

Richter, L., 2015. Fluid inclusion study on LCT pegmatites from Bikita, Zimbabwe craton-constraints on a magmatic-hydrothermal model. ECROFI XXIII Abstracts 7, 105.

Rickers, K., Thomas, R., Heinrich, W., 2006. The behavior of trace elements during the chemical evolution of the H_2O-, B-, and F-rich granite-pegmatite-hydrothermal system at Ehrenfriedersdorf, Germany: a SXRF study of melt and fluid inclusions. Miner. Depos. 41, 229–245. https://doi.org/10.1007/s00126-006-0057-7.

Roda-Robles, E., Pesquera, A., Velasco, F., 1995. Micas of the muscovite-lepidolite series from the Fregeneda pegmatites (Salamanca, Spain). Mineral. Petrol. 55, 145–157. https://doi.org/10.1007/BF01162585.

Samson, I.M., Williams-Jones, A.E., Ault, K.M., Gagnon, J.E., Fryer, B.J., 2008. Source of fluids forming distal Zn-Pb-Ag skarns: Evidence from laser ablation-inductively coupled plasma-mass spectrometry analysis of fluid inclusions from El Mochito. Honduras. Geology 36 (12), 947–950. https://doi.org/10.1130/G25214A.1.

Sigoyer, J.D., Vanderhaeghe, O., Duchêne, S., Billerot, A., 2014. Generation and emplacement of Triassic granitoids within the Songpan Ganze accretionary-orogenic wedge in a context of slab retreat accommodated by tear faulting, Eastern Tibetan plateau China. J. Asian Earth Sci. 88, 192–216. https://doi.org/10.1016/j.jseaes.2014.01.010.

Simmons, W.B., Webber, K.L., 2008. Pegmatite genesis: state of the art. Eur. J. Mineral. 20, 421–438. https://doi.org/10.1127/0935-1221/2008/0020-1833.

Sirbescu, M.L.C., Krukowski, E.G., Schmidt, C., Thomas, R., Samson, I.M., Bodnar, R.J., 2013. Analysis of boron in fluid inclusions by microthermometry, laser ablation ICP-MS, and Raman spectroscopy: applications to the Cryo-Genie Pegmatite, San Diego County, California USA. Chem. Geol. 342, 138–150. https://doi.org/10.1016/j.chemgeo.2013.01.014.

Steele-MacInnis, M., 2018. Fluid inclusions in the system H_2O-NaCl-CO_2: An algorithm to determine composition, density and isochore. Chem. Geol. 498, 31–44. https://doi.org/10.1016/j.chemgeo.2018.08.022.

Sterner, S.M., Hall, D.L., Bodnar, R.J., 1988. Synthetic fluid inclusions. V. Solubility relations in the system NaCl-KCl-H_2O under vapor-saturated conditions. Geochim. Cosmochim. Acta 52 (5), 989–1005. https://doi.org/10.1016/0016-7037(88)90254-2.

Stewart, D.B., 1978. Petrogenesis of lithium-rich pegmatites. Am. Mineral. 63, 970–980.

Thomas, R., Davidson, P., 2016. Revisiting complete miscibility between silicate melts and hydrous fluids, and the extreme enrichment of some elements in the supercritical state — consequences for the formation of pegmatites and ore deposits. Ore Geol. Rev. 72, 1088–1101. https://doi.org/10.1016/j.oregeorev.2015.10.004.

Van Daele, J., Hulsbosch, N., Dewaele, S., Boiron, M.C., Piessens, K., Boyce, A., Muchez, P., 2018. Mixing of magmatic-hydrothermal and metamorphic fluids and the origin of peribatholitic Sn vein-type deposits in Rwanda. Ore Geol. Rev. 101, 481–501. https://doi.org/10.1016/j.oregeorev.2018.07.020.

Weislogel, A.L., Graham, S.A., Chang, E.Z., Wooden, J.L., Gehrels, G.E., 2010. Detrital zircon provenance from three turbidite depocenters of the Middle-Upper Triassic Songpan-Ganzi complex, central China: record of collisional tectonics, erosional exhumation, and sediment production. Geol. Soc. Am. Bull. 122, 2041–2062. https://doi.org/10.1130/B26606.1.

Xu, Z., Fu, X., Wang, R., Li, G., Zheng, Y., Zhao, Z., Lian, D., 2020. Generation of lithium-bearing pegmatite deposits within the Songpan-Ganze orogenic belt. East Tibet. Lithos 354–355, 105281. https://doi.org/10.1016/j.lithos.2019.105281.

Yuan, Y., Moore, L.R., McAleer, R.J., Yuan, S., Ouyang, H., Belkin, H.E., Mao, J., Sublett, D.M., Bodnar, R.J., 2021. Formation of miarolitic-class, segregation-type pegmatites in the Taishanmiao batholith, China: The role of pressure fluctuations and volatile exsolution during pegmatite formation in a closed, isochoric system. Am. Mineral. 106 (10), 1559–1573. https://doi.org/10.2138/am-2021-7637.

Zajacz, Z., Halter, W.E., Pettke, T., et al., 2008. Determination of fluid/melt partition coefficients by LA-ICPMS analysis of co-existing fluid and silicate melt inclusions: Controls on element partitioning. Geochim. Cosmochim. Acta 72, 2169–2197. https://doi.org/10.1016/j.gca.2008.01.034.

Zhao, H., Chen, B., Huang, C., Bao, C., Yang, Q., Cao, R., 2022. Geochemical and Sr–Nd–Li isotopic constraints on the genesis of the Jiajika Li-rich pegmatites, eastern Tibetan Plateau: implications for Li mineralization. Contrib. Miner. Petrol. 177 (1), 1–16. https://doi.org/10.1007/s00410-021-01869.